PCCP

Accepted Manuscript

ROYAL SOCIETY OF CHEMISTRY

www.rsc.org/pccp

Journal Name

RSCPublishing

ARTICLE

An old workhorse for new applications: $Fe(dpm)_3$ as precursor for low-temperature PECVD of iron(III) oxide

Cite this: DOI: 10.1039/x0xx00000x

Received 00th January 2012,
Accepted 00th January 2012

DOI: 10.1039/x0xx00000x

www.rsc.org/

G. Carraro[a,*], C. Maccato[a,*], A. Gasparotto[a], D. Barreca[b], M. Walter[c,d], L. Mayrhofer[c,d], M. Moseler[c,d], A. Venzo[b], R. Seraglia[b], C. Marega[a]

An iron(III) β-diketonate complex, $Fe(dpm)_3$ (Hdpm = 2,2,6,6-tetramethyl-3,5-heptanedione) has been investigated as a potential precursor for the plasma enhanced chemical vapor deposition (PECVD) of iron(III) oxide nanomaterials. Thanks to a joint experimental–theoretical approach, $Fe(dpm)_3$ spectroscopic properties, spin state, thermal behavior and fragmentation pathways have been carefully analysed, obtaining an excellent agreement between simulation and experiment. Preliminary PECVD tests evidenced the possibility of obtaining pure and homogeneous Fe_2O_3 deposits with controlled nano-organization at temperatures as low as 100°C, even on flexible plastic substrates. The present results open intriguing perspectives for the exploitation of $Fe(dpm)_3$ as an efficient molecular source for the preparation of nanostructured iron(III) oxides to be used in energetics and gas sensing applications.

Introduction

Iron oxides and, in particular, Fe_2O_3, are attractive functional materials thanks to their abundance, easy accessibility to different polymorphs and wide range of chemico-physical properties.[1-5] The possibility of controlling their structure at the nano-scale, resulting in a variety of systems encompassing thin films, nanolamellae, nanorods and ordered nanoarrays, has significantly enlarged their utilization spectrum, ranging from magnetic recording media, gas sensors, heterogeneous (photo)catalysts, and, more recently, anodes in photoelectrochemical (PEC) cells for H_2O splitting.[6-18] Among the available synthetic routes, plasma enhanced chemical vapor deposition (PECVD) is a versatile technique for the preparation of supported iron oxide materials with a unique control on nanoscale organization even on large-area substrates.[18-21] Compared with other vapor phase approaches, a strategic advantage of PECVD lies in the potential of synthesizing crystalline deposits at low temperatures (eventually down to the room one) thanks to the exploitation of *non-equilibrium* cold plasmas.[19]

A key issue for the development of an efficient and reproducible PECVD process is the availability of molecular precursors with well-defined chemico-physical properties, such as high volatility, stability against air and moisture, low toxicity and clean fragmentation pattern.[22,23] As a consequence, the design and development of suitable precursors represent an important research area, integrating molecular chemistry and materials science.[24,25] In this regard, a strategic tool is offered by a synergistic experimental–theoretical approach, providing key indications in the design and selection of PECVD precursors with suitable features.[23,26,27] So far, various molecular compounds have been tested as iron sources in thermal CVD processes (such as Fe alkoxides, *β*-diketonates, ferrocenes and carbonyls),[5,10,11,22,28] but the peculiar PECVD requirements have further restricted the number of possible compounds. In fact, the characteristics of *non-equilibrium* plasmas and low deposition temperatures characterizing PECVD routes, as well as safety issues, have to be carefully considered.[29] As a matter of fact, the most used precursor in PECVD routes to Fe_2O_3 materials is $Fe(CO)_5$,[11,16,18,28,30] but its flammability, toxicity and very high vapor pressure prevent from a fine control on the growth process and make the availability of alternative sources a stringent requirement. An attractive option for the development of improved CVD precursors involves the introduction of fluorinated ligands, that results in stable adducts with enhanced volatility.[22,23,31] Yet, in the case of PECVD processes, fluorinated compounds result in the ubiquitous generation of F-containing radicals, affecting the material composition and functional behavior.[20,21] Hence, if fluorine-free iron oxides are desired, the use of such precursors has necessarily to be discarded.

Basing on the above observations, a possible option involves the strike-back of "old workhorses". Non-toxic, non-fluorinated and environmentally safe metal *β*-diketonates have been widely applied in the fabrication of oxide materials, thanks to their ambient stability and appreciable volatility.[25,32,33] In addition, *β*-diketonates generally show a clean fragmentation,[24] a key advantage in PECVD processes. Among various *β*-diketonates, $Fe(dpm)_3$ (Hdpm = 2,2,6,6-tetramethyl-3,5-heptanedione) (Fig. 1) has demonstrated an improved thermal stability and lower tendency to hydration and polymerization than common acetylacetonates, thanks to the steric hindrance of the bulky substituents.[25] As a matter of fact, $Fe(dpm)_3$ has been previously used only in thermal CVD and atomic layer deposition (ALD) processes.[34,35] Nevertheless, to the best of our knowledge, a rational characterization of this compound as a CVD precursor, with particular regard to its use in PECVD processes, has not yet been reported up to date.

In the present work, $Fe(dpm)_3$ has been studied by a joint experimental–theoretical approach, in order to investigate its

spectroscopic properties, thermal behavior and possible fragmentation pathways. In addition, $Fe(dpm)_3$ has been tested in PECVD processes, yielding nanostructured deposits at a deposition temperature as low as 100°C, even on thermally labile substrates. In perspective, this feature is of strategic interest for the fabrication of a variety of next-generation technological devices on flexible plastics. As a matter of fact, the present results are very attractive not only from a fundamental point of view, but also for the potential application of the developed iron oxide materials in photocatalytic/photoelectrochemical H_2 generation and gas sensing.

Experimental

$Fe(dpm)_3$ synthesis

The synthesis of $Fe(dpm)_3$ was performed through a modification of the procedure reported by Hammond *et al.*.[36] In particular, a NaOH solution (2.15 g, 54 mmol, in 10 mL of deionized H_2O) has been added to a $FeCl_3$ solution (Aldrich®, 98%; 2.92 g, 18 mmol, in 15 ml of deionized H_2O), resulting in a color change from light yellow to dark red. Subsequently, a solution of Hdpm *(*ABCR®, 98+%; 9.9 g, 0.54 mmol in 25 ml of ethanol, Aldrich®, 98%) was added dropwise to the previous aqueous mixture. The obtained solution was maintained under vigorous stirring and heated at 60°C for 1 hour. After reaction the solution turned into a light red color and was characterized by the presence of a precipitate, which was recovered by filtration and dried, yielding a dark orange solid (yield of the overall synthesis = 90%). The compound was soluble in various solvents, such as dichloromethane, 1,2-dichloroethane, acetone and alcohols.

$Fe(dpm)_3$ characterization

The complex melting point (m.p.) was measured in air by a FALC melting point device at atmospheric pressure, yielding m.p. = 165°C.[37] Elemental analyses were carried out by a Fisons Carlo Erba EA1108 apparatus (CHNS version). Calcd. for $C_{33}H_{57}O_6Fe$: C, 65.4%; H, 9.4%. Found: C, 65.4%; H, 9.5%.

Nuclear magnetic resonance (NMR) spectra were recorded at 25°C on $CDCl_3$ solutions of the target compound (50 mg/ml) by a Bruker DMX-400 instrument equipped with a 9.4 T magnet. Under these conditions, the basic frequencies for the ^1H and ^{13}C nuclei are 400.13 and 100.61 MHz, respectively. The chemical shift values were referenced to internal Me_4Si. Owing to the high spread of chemical shift values due to the paramagnetic interactions, the sweep width of 75 KHz for proton and carbon were used (the greatest values allowed for the available hardware), and spectral regions between –1000 and + 1000 ppm were stepwise exploited. The aring Bruker pulse program was used to avoid the acoustic ringing usually associated with large spectral windows (see the Electronic Supplementary Information (ESI†) for further data).

The magnetic moment expressed in Bohr magneton units, μ, was obtained through three independent determinations of the magnetic susceptibility, χ_m, performed on a Sherwood Scientific MSB MK-I magnetic balance at 25°C.

A Cary 50 spectrophotometer (Varian) was used for UV-Vis analyses (spectral bandwidth = 1 nm). Measurements were carried out on ethanol solutions (10^{-4} M) of $Fe(dpm)_3$ using quartz couvettes (optical path = 0.5 cm).

Thermogravimetric and differential scanning calorimetry (TGA and DSC) analyses were performed at ambient pressure under synthetic air (sample weight = 6.3 mg; heating rate = 10°C × min^{-1}) using an SDT2960 apparatus (TAinstruments). Isothermal investigations were carried out in air.

Electrospray ionization-mass spectrometry (ESI-MS) was performed using a LCQ Deca ion trap instrument (ThermoFisher), operating in positive ion modes. The used entrance capillary temperature and voltage were set at 250°C and 4 kV, respectively. A 10^{-6} M solution of the target compound in water/methanol (50:50, v:v) was introduced by direct infusion using a syringe pump (flow rate = 10 $\mu L \times min^{-1}$. MS/MS experiments were performed by applying a supplementary Radio Frequency (RF) voltage to the end caps of the ion trap (5 V peak-to-peak).

Simulation

The $Fe(dpm)_3$ electronic structure was studied by means of density functional theory (DFT). DFT calculations were performed within the grid projector augmented wave (GPAW) method.[38] The smooth part of the Kohn-Sham wave functions was represented on real space grids with spacing h = 0.2 Å, whereas 0.1 Å grid spacing was used to represent the smooth density. The simulation cell was chosen large enough to contain a more than 4.0 Å wide vacuum region around the $Fe(dpm)_3$ complex. Dirichlet boundary conditions for the wave functions were applied. These settings have been checked for convergence and the results can be considered as the large basis set limit. The exchange-correlation energy was approximated in the generalized gradient approximation (GGA) as devised by Perdew, Burke, and Ernzerhof (PBE).[39,40] The correct description of the complex electronic structure and spin state made it necessary to adopt the PBE+U method, which describes the localized iron *d*-orbitals adequately.[40,41] An effective U=4 eV was used, that has been successful in the description of complexes in the same family.[41] The structures have been relaxed without symmetry constraints until the forces were lower than 0.01 eV/Å. Vibrational spectra and IR intensities were obtained from a finite difference approximation.[42] Optical spectra were calculated within time-dependent DFT using the linear response formulation.[43]

PECVD experiments

Si(100) substrates (1.5×1.5 cm^2) were purchased from MEMC® (Merano, Italy) and cleaned prior to deposition by iterative dipping in a sulphonic detergent solution, isopropylic alcohol and deionized water, followed by drying under an Ar flow. Growth experiments were carried out in Ar/O_2 plasmas (flow rates = 15 and 20 sccm, respectively), using a custom-built two-electrode radio frequency (RF, ν = 13.56 MHz) PECVD apparatus.[44] After preliminary optimization experiments, the total pressure, deposition time and RF-power were kept constant at 1.0 mbar, 60 min and 20 W, respectively. A deposition temperature of 100°C was adopted. $Fe(dpm)_3$ powders, introduced in an external glass vessel, were vaporized at 130°C by means of an oil bath, and its vapor was transported into the reaction chamber by an Ar flow (rate = 60 sccm). Gas lines were heated to 160°C to prevent detrimental precursor condensation phenomena. As a proof of concept, flexible polyester sheets were also used as growth substrates.

Material characterization

X-ray diffraction (XRD) measurements were run in reflection mode on a Dymax-RAPID X-ray microdiffractometer using CuKα radiation (λ = 1.5418 Å).

Field emission-scanning electron microscopy (FESEM) micrographs were collected by a Zeiss SUPRA 40VP instrument, using primary beam acceleration voltages of 10 kV.

X-ray photoelectron spectroscopy (XPS) measurements were performed on a Perkin-Elmer Φ5600ci spectrometer with a non-monochromatized AlKα source (hν=1486.6 eV) at pressures lower than 10^{-8} mbar. After a Shirley-type background subtraction, raw spectra were fitted by adopting Gaussian–Lorentzian peak shapes. Charging correction was performed by assigning a binding energy (BE) of 284.8 eV to the adventitious C1s signal.[45] The estimated uncertainty on BE values was ±0.2 eV.

Results and discussion

The calculated structure of the $Fe(dpm)_3$ complex is depicted in Fig. 1. Bond lengths and angles are in good agreement to the published crystal structure.[37] ^{1}H-NMR spectra of $Fe(dpm)_3$ were recorded in $CDCl_3$ (Fig. S1), revealing an intense and broad ($l.w_{1/2}$ ≈3 kHz) line at δ 13.04 attributed to the methyl protons, and a much less intense, broader one at ca. δ -22.8 ($l.w_{1/2}$ ≈8 kHz) attributed to the residual central proton of the dpm unit.[23] As expected, the ^{13}C resonances (Fig. S2) appeared at δ ≈45.9 ($l.w_{1/2}$ ≈8.5Hz) and ≈110 ($l.w_{1/2}$ ≈25 kHz) for CH_3 and CH carbons, respectively. No resonance was detected for the carbonyl C atoms, likely due to the extreme broadening induced by the paramagnetic centre. It is worthwhile noticing that the acquisition and assignment of NMR spectra of paramagnetic complexes is often difficult due to the strong interaction between nuclear and electronic moments, resulting in features with unusual resonance frequencies and broad lines (often several kHz), the effect being more pronounced in the proximity of the paramagnetic center.[46]

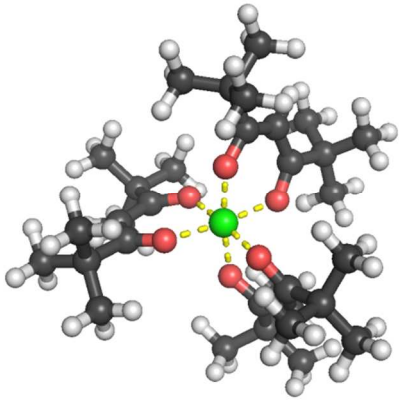

Fig. 1 Relaxed structure of $Fe(dpm)_3$. Color codes: Fe, green; O, red; C, black; H, white. The 2.04 Å Fe-O bonds are marked by yellow dashed lines (see also Table S1, ESI†).

As a matter of fact, the paramagnetic characteristics of the $Fe(dpm)_3$ molecule was further confirmed by magnetic moment measurements. The obtained value, 6.8±0.3 BM, indicating a strongly paramagnetic complex, was in excellent agreement with the moment predicted for a d^5 high-spin configuration (6.89 BM).[47] This phenomenon has been further confirmed by DFT calculations, where the d^5 high-spin configuration (S_z=5/2 state in units of ħ) was found to be 1.11 eV lower in energy than the low-spin S_z=1/2 state. Similar to the results obtained for other Fe^{III} complexes of the same family,[41] the PBE (U=0) approximation misleadingly predicted the lower spin state to be the ground state, possessing a lower energy of 0.06 eV with respect to the high-spin state. Only when the correction with finite U is applied, the low-spin state was found at a higher energy than the S_z=5/2 state, in agreement with magnetic moment measurements.
Further confirmation for the high-spin state of $Fe(dpm)_3$ was obtained from the optical and IR spectra (Fig. 2), that showed a good agreement between simulated and experimental data, and were in line with previous literature reports.[24] The IR spectra of the two spin states were nearly indistinguishable and agreed to a good extent with experimental data (see also Table S2, ESI†, for a detailed assignment of vibrational lines). In contrast, the corresponding optical spectra were clearly different due to their strong dependence on the electronic structure,[48] and only the simulated high-spin state spectrum was in agreement with the experimental one. The large wavelength peak at λ≈450 nm was completely missing in the simulated low-spin spectrum, but appeared as a broad shoulder in the experimental one. Analysis of the optical transitions revealed that this peak was mainly due to transitions from occupied C and O orbitals to the empty *d* orbitals in the minority spin manifold (compare the projected density of states in Fig. S3). A very similar peak was found in complexes of the same family.[41] The high-spin spectrum showed also a small shoulder around 350 nm followed by the steep rise towards small wavelengths, in accordance with experimental data.
The knowledge of the precursor thermal behaviour is of key importance to develop controlled and reproducible CVD and PECVD growth processes. TGA/DSC analyses (Fig. 3a) revealed very similar results for freshly synthesized and aged sample batches.

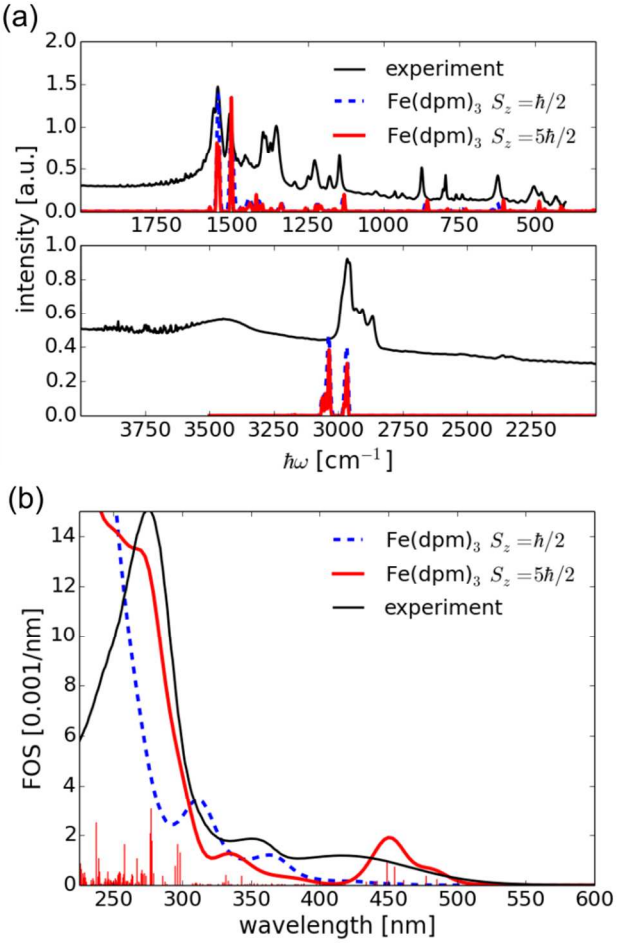

Fig. 2 (a) Comparison of experimental and simulated IR spectra of $Fe(dpm)_3$. (b) Theoretical folded oscillator strengths (FOS) of $Fe(dpm)_3$ compared to the experimental UV-Vis spectrum. The theoretical spectrum is broadened by Gaussians of 10 nm width and the experimental spectrum is scaled for a better fitting to the theoretical one.

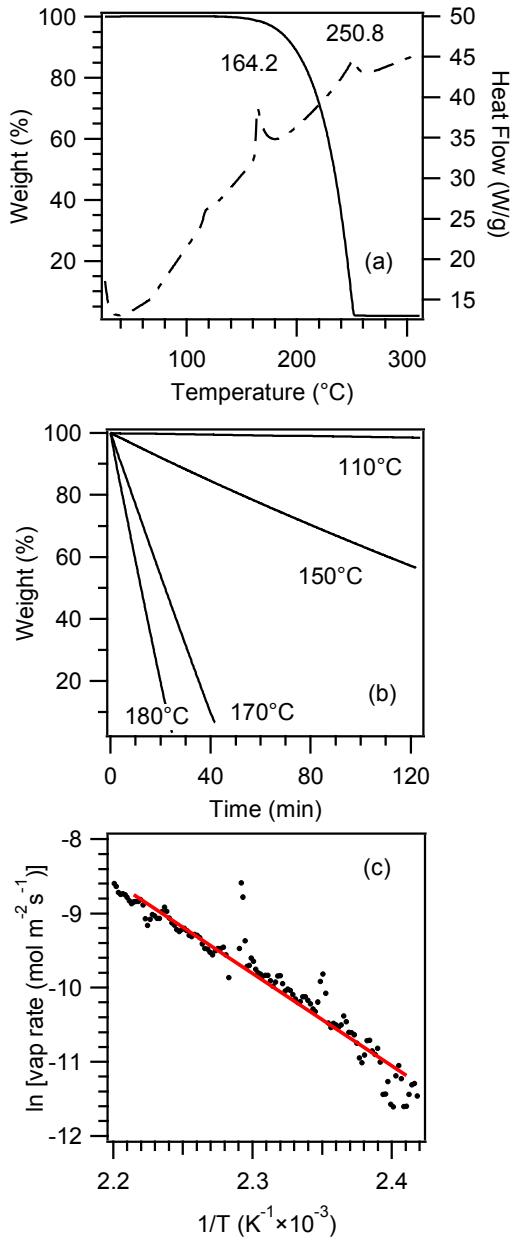

Fig. 3 (a) TGA (solid) and DSC (dashed) profiles; (b) isothermal studies carried out at different temperatures; (c) Arrhenius plot for the vaporization of $Fe(dpm)_3$ in air.

For temperatures higher than 150°C, the recorded data showed an appreciable weight loss, corresponding to a single-step powder vaporization resulting in a residual weight close to zero for T > 250°C, highlighting the quantitative sublimation of the target compound.The knowledge of the precursor decomposition mechanism in CVD experiments, and in particular the sequence of the ligand bond dissociation, is still rather limited, despite it is expected to have a direct impact on the final material properties.[24] In addition, DSC analysis enabled to identify two endothermic peaks at 164.2 and 250.8°C, due to $Fe(dpm)_3$ melting and vaporization, respectively.[37] Isothermal analyses (Fig. 3b) carried out at temperatures between 110 and 180°C revealed a constant weight loss for time periods up to 2 h, enabling to rule out the occurrence of detrimental decomposition phenomena. Fig. 3c displays the logarithmic dependence of vaporization rate on the inverse of the absolute temperature. In the investigated range, a linear trend was observed, indicating a vaporization process free from undesired side reactions. Basing on the Clausius–Clapeyron equation, the apparent molar vaporization enthalpy could be estimated by the slope of the experimental curve, yielding $\Delta H_{vap} = 103 \pm 4$ kJ × mol^{-1} = 1.07±0.04 eV. This result, in line with previously reported values for first generation iron β-diketonates compounds,[25,31] pointed out to the occurrence of a pure vaporization without any premature decomposition, a key issue for achieving a constant precursor mass transport in CVD/PECVD processes.

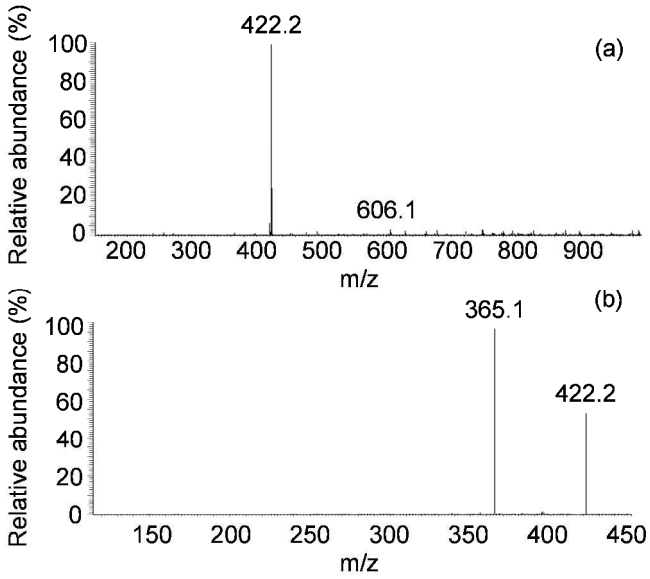

Fig. 4 (a) ESI-MS spectrum of $Fe(dpm)_3$ in water/methanol solution. (b) MS/MS spectrum of $Fe(dpm)_2^+$ ion.

In order to shed light on the first steps of precursor fragmentation, ESI-MS and MS/MS studies have been carried out. The ESI-MS spectrum of $Fe(dpm)_3$ is shown in Fig. 4a. The ion at m/z = 606.1 originates from the protonation of $Fe(dpm)_3$, whereas the one at m/z = 422.2 corresponds to $Fe(dpm)_2^+$, indicating the loss of a dpm unit as the initial fragmentation step. In order to achieve more detailed information, further MS/MS experiments on the fragments of the ESI-MS spectrum were attempted. These were not possible for the protonated complex due to its very low abundance, but were carried out on the ion at m/z = 422.2, leading to the spectrum reported in Fig. 4b. The spectrum is characterized by the presence of the sole ion at m/z = 365.1, corresponding to the loss of a $C(CH_3)_3$ radical from $Fe(dpm)_2^+$. Overall, these results highlight the occurrence of a very clean fragmentation pattern.

The initial fragmentation energetic, obtained by DFT calculations, is sketched in Fig. 5. The energy needed to remove a neutral dpm unit from $Fe(dpm)_3$ is 2.27 eV [reaction (1)], whereas the removal of an anionic dpm unit needs 6.15 eV and is thus unlikely. This suggests that a neutral precursor molecule should decompose according to the reaction:

$$Fe(dpm)_3 \rightarrow Fe(dpm)_2^* + dpm^* \quad (1)$$

where the asterisk denotes a radical (*i.e.*, an unpaired electron). Although the ESI-MS experimental conditions are rather different from those of PE-CVD experiments, it might be argued that, during PECVD processes, free electrons present in the plasmas could be attached to $Fe(dpm)_3$ (electron affinity is 1.96 eV). Interestingly, in this case the extraction of dpm^- is strongly favoured in the reaction:

$Fe(dpm)_3^- \rightarrow Fe(dpm)_2^* + dpm^-$ (2)

which requires 1.60 eV only. On the other hand, it is well known that the substrate will be negatively charged during the PECVD process,[19] thus attracting only positive ions. Ionizing $Fe(dpm)_3$ needs a rather high energy (6.85 eV), but should be possible under the typically used PECVD conditions.

Similar to reaction (2), the positive charge present on the $Fe(dpm)_3$ fragment located at *m/z* = 606.1 facilitates the abstraction of a dpm unit as compared to the neutral molecule *via*

$Fe(dpm)_3^+ \rightarrow Fe(dpm)_2^+ + dpm^*$ (3)

which needs 1.92 eV only. This is in agreement with the fact that $Fe(dpm)_2^+$ is the main fragment observed in the ESI-MS spectrum and that no polynuclear species have been detected under these experimental conditions.

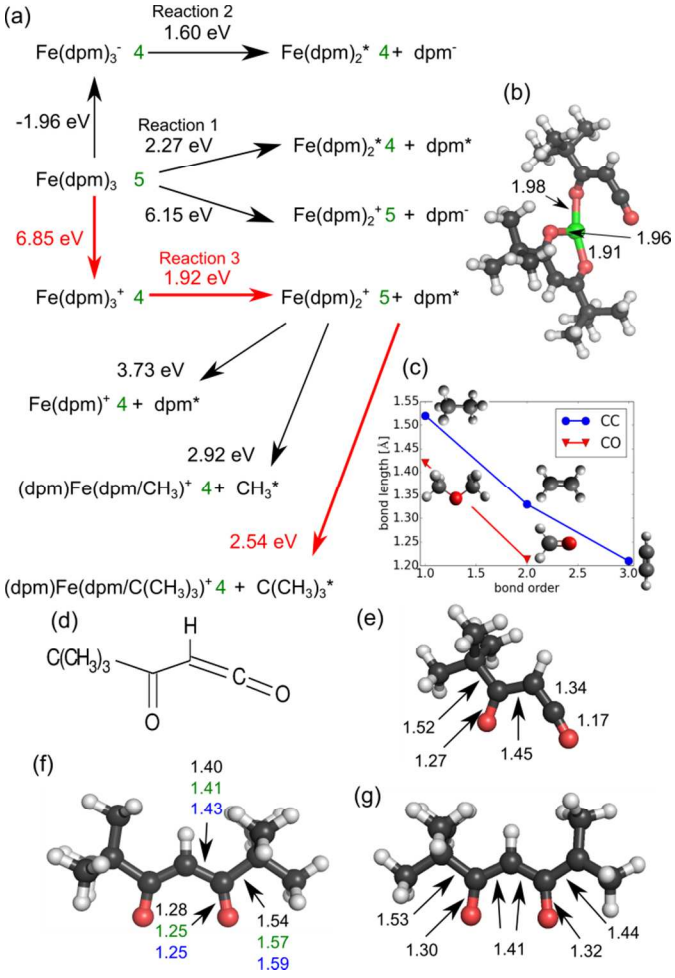

Fig. 5 (a) Fragmentation energetics of $Fe(dpm)_3$. The proposed path is marked by red arrows. The asterisks mark neutral radicals. For each fragment, the lowest energy spin state in units of $\hbar/2$ is denoted by green numbers. (b) Relaxed structure of $[Fe(dpm)_2]^+$ with a $C(CH_3)_3$ group removed. Color codes: Fe, green; O, red; C, black; H, white. (c) Correlation between bond length and bond order in CC and CO bonds (see ESI† for details). (d,e) Structure of the dpm unit with a $C(CH_3)_3$ group removed. In (e, relevant bond distances are marked. (f) The dpm unit with bond lengths within $Fe(dpm)_3$ (black numbers), isolated dpm (green numbers) and isolated $[dpm]^-$ (blue numbers) and (g) dpm with a CH_3 group removed. All bond lengths are given in Å.

Calculations showed that a removal of a further dpm unit from $Fe(dpm)_2^+$ would require 3.73 eV, a value higher than 2.92 eV, the energy input necessary to abstract a CH_3 group. However, the abstraction of a $C(CH_3)_3$ group requires an even lower energy (2.54 eV). The reason for this phenomenon can be rationalized from Fig. 5b, showing the relaxed configuration after abstraction, where the central iron atom is only connected to a single oxygen atom of the involved dpm unit. Accordingly, the dpm fragment is bound by 2.00 eV only, as compared to the 3.73 eV before. The missing $C(CH_3)_3$ group enables a strong relaxation, with variations of the bond lengths in the fragment (Figs. 5d,e). Bond length analysis in the relaxed dpm fragment revealed that the oxygen atoms form double bonds with the carbon ones, forcing a rearrangement of the bonds around the central C atom, *i.e.* a single bond with 1.45 Å and a double bond with 1.34 Å (the correlation between CC and CO bond lengths and the corresponding bond order is displayed in Fig. 5c, see ESI† for further details). A similar rearrangement does not occur when only a methyl group is abstracted as can be seen by a comparison of the bond lengths in Figs. 5f and 5g. In this case the chemical structure of the dpm unit remains almost intact, irrespective of the charge state and iron atom presence

The potential of $Fe(dpm)_3$ as a PECVD precursor was tested by carrying out preliminary growth processes on Si(100) and polymeric substrates, with particular focus on the possibility of obtaining iron(III) oxide nanomaterials at low deposition temperatures. Remarkably, at only 100°C, a temperature even lower than that required by precursor vaporization, uniform orange/red deposits were obtained (Fig. 6a), characterized by a remarkable adhesion to the substrate, as confirmed by the scotch tape test. As a matter of fact, the deposition of a Fe_2O_3 even on a flexible polymeric substrate is of great importance, since it can disclose new applicative frontiers in the fabrication and processing of iron oxide nanomaterials.

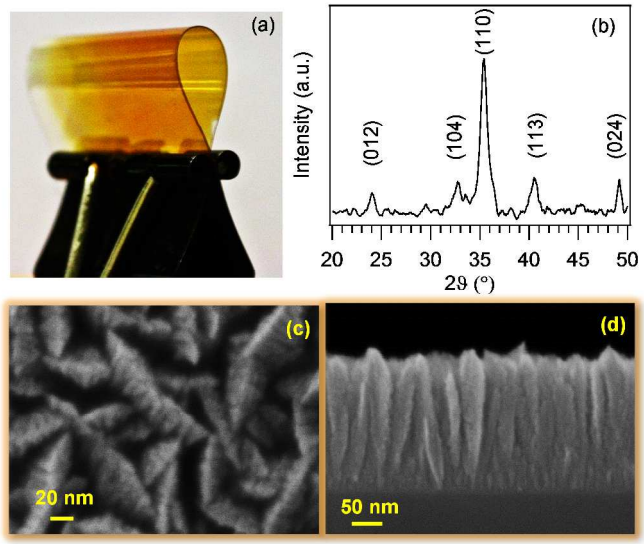

Fig. 6 (a) Digital photograph of a Fe_2O_3 deposit on a flexible polymeric substrate obtained at 100°C. (b) XRD pattern, (c) plane view and (d) cross sectional FESEM micrographs of a Fe_2O_3 specimen grown at 100°C on Si(100).

The system crystallinity was studied by XRD (Fig. 6b), that indicated the formation of single-phase *hematite* (α-Fe_2O_3) deposits, considering that only reflections at 2ϑ = 24.1°, 33.0°, 35.7°, 40.9° and 49.5° were observed.[49] It is also important to notice that the material showed a preferential orientation along the (110) direction, probably due to the unique *non-equilibrium* conditions

characterizing cold plasmas. Due to the anisotropic conductivity of α-Fe_2O_3, this phenomenon can result in improved functional performances, especially in photoelectrochemical applications.[12]
In order to validate the present approach, the systems morphology has been studied by FESEM (Figs. 6c,d). The deposit showed a well-defined and homogeneous nano-organization, characterized by the presence of elongated leaf-like structures (width = 20 nm), growing perpendicular to the Si(100) substrate surface. Such kind of nanostructures, characterized by a large surface area and a short Debye length, are very interesting in view of possible applications such as PEC anodes and solid state gas sensors.[7,14,15] A further important issue concerns the material purity and chemical composition. To this regard, Fig. 7 shows a representative wide-scan XPS spectrum, which is dominated by iron and oxygen photopeaks. The presence of carbon can be related to adventitious surface contamination upon atmospheric exposure, since the C1s signal fell to a noise level after a few minutes of Ar^+ sputtering.

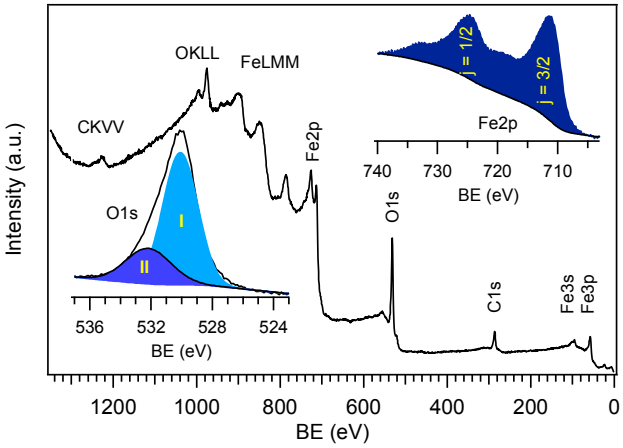

Figure 7. Surface XPS survey of a Fe_2O_3 specimen deposited at 100°C on Si(100). The O1s and Fe2p photoelectron peaks are also displayed as insets.

The O1s peak could be decomposed into two bands, located at BE = 530.0 (I) and 531.8 eV (II), that were attributed to lattice oxygen in iron(III) oxide and surface hydroxyls/carbonates arsing from air exposure, respectively.[2,20,50] The Fe2p peak shape and position [BE($Fe2p_{3/2}$) = 711.1 eV], along with the energy separation between spin–orbit components [Δ(BE) = 13.5 eV], was consistent with the formation of iron(III) oxide free from other Fe oxidation states.[2,18,20,50]
These results clearly confirm the possibility of successfully exploiting $Fe(dpm)_3$ as a precursor for the PECVD of pure Fe_2O_3 nanosystems even at low deposition temperatures.

Conclusions

In the present work, $Fe(dpm)_3$ has been investigated as iron source for the PECVD growth of iron oxide nanostructures. A rational characterization of the precursor structural, electronic, thermal and fragmentation behavior, enabled by a joint experimental and theoretical approach, highlighted its favourable properties for application in PECVD processes. In particular, this complex, that can be easily prepared on open benches, showed a high stability to air/moisture and a single-step vaporization, that, along with the clean fragmentation pathway, represent key advantages for its use in PECVD. Calculations suggested that the first fragmentation consists in the abstraction of a dpm unit from a charged $Fe(dpm)_3$, followed by a removal of a $C(CH_3)_3$ group.
PECVD experiments starting from $Fe(dpm)_3$ resulted in the synthesis of α-Fe_2O_3 nanodeposits characterized by an high purity and a controlled nano-organization. In addition, the possibility of depositing at temperature as low as 100°C, allowed Fe_2O_3 growth even on thermally labile polymeric substrates, an important issue in view of their ultimate technological application.
On the basis of the presented results, the exploitation of $Fe(dpm)_3$ for the preparation of iron oxide deposits to be tested as photocatalysts for H_2 generation, PEC anodes and gas sensors is already under way.

Acknowledgements

The authors kindly acknowledge the financial support under the FP7 project "SOLAROGENIX" (NMP4-SL-2012-310333), as well as Padova University ex-60% 2012-2014 projects, grant n°CPDR132937/13 (SOLLEONE), and Regione Lombardia-INSTM ATLANTE projects. Thanks are also due to Prof. M. Zecca (Padova University, Italy), Prof. E. Bontempi (Brescia University, Italy), Dr. N. Tiso and Dr. R. Saini (Padova University, Italy) for valuable assistance in precursor and specimen characterization. Computational resources from FZ-Jülich are also gratefully acknowledged.

Notes and references

[a] *Department of Chemistry - Padova University and INSTM - 35131 Padova, Italy. E-mail: giorgio.carraro@unipd.it (G.C.); chiara.maccato@unipd.it (C.M.).*
[b] *CNR-IENI and INSTM - Department of Chemistry - Padova University - 35131 Padova, Italy.*
[c] *Fraunhofer Institute for Mechanics of Materials - 79108 Freiburg, Germany.*
[d] *Freiburg Materials Research Center - Freiburg University - 79104 Freiburg, Germany. E-mail: michael.walter@fmf.uni-freiburg.de (M.W.).*

† Electronic Supplementary Information (ESI) available: [NMR characterization and computational results for $Fe(dpm)_3$].

1. P. Tartaj, M. P. Morales, T. Gonzalez-Carreño, S. Veintemillas-Verdaguer and C. J. Serna, *Adv. Mater.*, 2011, **23**, 5243-5249.
2. G. Carraro, C. Maccato, E. Bontempi, A. Gasparotto, O. I. Lebedev, S. Turner, L. E. Depero, G. Van Tendeloo and D. Barreca, *Eur. J. Inorg. Chem.*, 2013, **2013**, 5454-5461.
3. R. M. Cornell and U. Schwertmann, *The Iron Oxides: Structures, Properties, Reactions, Occurences and Uses*, Wiley-VCH Verlag, Weinheim, 2003.
4. L. Machala, J. i. Tuček and R. Zbořil, *Chem. Mater.*, 2011, **23**, 3255-3272.
5. M. K. Singh, Y. Yang and C. G. Takoudis, *J. Electrochem. Soc.*, 2008, **155**, D618-D623.
6. S. Xiong, J. Xu, D. Chen, R. Wang, X. Hu, G. Shen and Z. L. Wang, *CrystEngComm*, 2011, **13**, 7114-7120.
7. J. Brillet, M. Grätzel and K. Sivula, *Nano Lett*, 2010, **10**, 4155-4160.
8. K. Sivula, F. Le Formal and M. Grätzel, *ChemSusChem*, 2011, **4**, 432-449.
9. G. Carraro, C. Maccato, A. Gasparotto, T. Montini, S. Turner, O. I. Lebedev, V. Gombac, G. Adami, G. Van Tendeloo, D. Barreca and P. Fornasiero, *Adv. Funct. Mater.*, 2014, **24**, 372-378.
10. E.-T. Lee, G.-E. Jang, C. K. Kim and D.-H. Yoon, *Sens. Actuators B*, 2001, **77**, 221-227.

11. M. Marelli, A. Naldoni, A. Minguzzi, M. Allieta, T. Virgili, G. Scavia, S. Recchia, R. Psaro and V. Dal Santo, *ACS Appl. Mater. Interfaces*, 2014, **6**, 11997-12004.
12. W. D. Chemelewski, N. T. Hahn and C. B. Mullins, *J. Phys. Chem. C*, 2012, **116**, 5255-5261.
13. G. Carraro, R. Sugrañez, C. Maccato, A. Gasparotto, D. Barreca, C. Sada, M. Cruz-Yusta and L. Sánchez, *Thin Solid Films*, 2014, **564**, 121-127.
14. L. Wang, T. Fei, Z. Lou and T. Zhang, *ACS Appl. Mater. Interfaces*, 2011, **3**, 4689-4694.
15. X. Li, W. Wei, S. Wang, L. Kuai and B. Geng, *Nanoscale*, 2011, **3**, 718-724.
16. P. Synek, O. Jašek, L. Zajíčková, B. David, V. Kudrle and N. Pizúrová, *Mater. Lett.*, 2011, **65**, 982-984.
17. I.-S. Lim, G.-E. Jang, C. K. Kim and D.-H. Yoon, *Sens. Actuators B*, 2001, **77**, 215-220.
18. A. Mettenbörger, T. Singh, A. P. Singh, T. T. Järvi, M. Moseler, M. Valldor and S. Mathur, *Int. J. Hydrogen Energy*, 2014, **39**, 4828-4835.
19. A. Gasparotto, D. Barreca, D. Bekermann, A. Devi, R. A. Fischer, C. Maccato and E. Tondello, *J. Nanosci. Nanotechnol.*, 2011, **11**, 8206-8213.
20. G. Carraro, A. Gasparotto, C. Maccato, E. Bontempi, O. I. Lebedev, S. Turner, C. Sada, L. E. Depero, G. Van Tendeloo and D. Barreca, *RSC Adv.*, 2013, **3**, 23762-23768.
21. A. Gasparotto, D. Barreca, D. Bekermann, A. Devi, R. A. Fischer, P. Fornasiero, V. Gombac, O. I. Lebedev, C. Maccato, T. Montini, G. Van Tendeloo and E. Tondello, *J. Am. Chem. Soc.*, 2011, **133**, 19362-19365.
22. G. Fornalczyk, M. Valldor and S. Mathur, *Cryst. Growth Des.*, 2014, **14**, 1811-1818.
23. D. Barreca, G. Carraro, A. Devi, E. Fois, A. Gasparotto, R. Seraglia, C. Maccato, C. Sada, G. Tabacchi, E. Tondello, A. Venzo and M. Winter, *Dalton Trans.*, 2012, **41**, 149-155.
24. Y. Jiang, M. Liu, Y. Wang, H. Song, J. Gao and G. Meng, *J. Phys. Chem. A*, 2006, **110**, 13479-13486.
25. M. A. Siddiqi, R. A. Siddiqui and B. Atakan, *J. Chem. Eng. Data*, 2010, **55**, 2149-2154.
26. E. Fois, G. Tabacchi, D. Barreca, A. Gasparotto and E. Tondello, *Angew. Chem. Int. Ed.*, 2010, **49**, 1944-1948.
27. G. Tabacchi, E. Fois, D. Barreca and A. Gasparotto, *Int. J. Quantum Chem.*, 2014, **114**, 1-7.
28. A. P. Singh, A. Mettenbörger, P. Golus and S. Mathur, *Int. J. Hydrogen Energy*, 2012, **37**, 13983-13988.
29. A. Kafizas, C. J. Carmalt and I. P. Parkin, *Coord. Chem. Rev.*, 2013, **257**, 2073-2119.
30. B. J. Kim, E. T. Lee and G. E. Jang, *Thin Solid Films*, 1999, **341**, 79-83.
31. B. D. Fahlman and A. R. Barron, *Adv. Mater. Opt. Electr.*, 2000, **10**, 223-232.
32. O. Nilsen, H. Fjellvåg and A. Kjekshus, *Thermochim. Acta*, 2003, **404**, 187-192.
33. V. A. Varnek, I. K. Igumenov, P. A. Stabnikov and L. N. Mazalov, *J. Struct. Chem.*, 2001, **42**, 860-863.
34. M. Lie, K. Barnholt Klepper, O. Nilsen, H. Fjellvag and A. Kjekshus, *Dalton Trans.*, 2008, 253-259.
35. G. G. Condorelli, M. R. Catalano, E. Smecca, R. Lo Nigro and G. Malandrino, *Surf. Coat. Technol.*, 2013, **230**, 168-173.
36. G. S. Hammond, D. C. Nonhebel and C.-H. S. Wu, *Inorg. Chem.*, 1963, **2**, 73-76.
37. M. A. K. Ahmed, H. Fjellvåg, A. Kjekshus and D. S. Wragg, *Zeit. Anorg. All. Chem.*, 2013, **639**, 770-778.
38. J. J. Mortensen, L. B. Hansen and K. W. Jacobsen, *Phys. Rev. B*, 2005, **71**, 035109.
39. J. P. Perdew, K. Burke and M. Ernzerhof, *Phys. Rev. Lett.*, 1996, **77**, 3865-3868.
40. J. Enkovaara, C. Rostgaard, J. J. Mortensen, J. Chen, M. Dułak, L. Ferrighi, J. Gavnholt, C. Glinsvad, V. Haikola, H. A. Hansen, H. H. Kristoffersen, M. Kuisma, A. H. Larsen, L. Lehtovaara, M. Ljungberg, O. Lopez-Acevedo, P. G. Moses, J. Ojanen, T. Olsen, V. Petzold, N. A. Romero, J. Stausholm-Møller, M. Strange, G. A. Tritsaris, M. Vanin, M. Walter, B. Hammer, H. Häkkinen, G. K. H. Madsen, R. M. Nieminen, J. K. Nørskov, M. Puska, T. T. Rantala, J. Schiøtz, K. S. Thygesen and K. W. Jacobsen, *J. Phys. Cond. Mat.*, 2010, **22**, 253202.
41. M. Walter, T. Amann, K. Li, A. Kailer, J. Rühe and M. Moseler, *J. Phys. Chem. A*, 2013, **117**, 3369-3376.
42. D. Porezag and M. R. Pederson, *Phys. Rev. B*, 1996, **54**, 7830-7836.
43. M. Walter, H. Häkkinen, L. Lehtovaara, M. Puska, J. Enkovaara, C. Rostgaard and J. J. Mortensen, *J. Chem. Phys.*, 2008, **128**, 244101
44. D. Barreca, A. Gasparotto, E. Tondello, C. Sada, S. Polizzi and A. Benedetti, *Chem. Vap. Dep.*, 2003, **9**, 199-206.
45. D. Briggs and M. P. Seah, *Practical surface analysis: Auger and X-ray photoelectron spectroscopy*, John Wiley & Sons: New York, 2nd ed., 1990.
46. I. Bertini, C. Luchinat and G. Parigi, *Solution NMR of Paramagnetic Molecules: Applications to Metallobiomolecules and Models*, Elsevier, Amsterdam, 2001.
47. P. Atkins, T. Overton, J. Rourke, M. Weller, F. Armstrong and M. Hagerman, *Inorganic Chemistry*, 5th ed., Oxford University Press, Oxford (UK), 2010.
48. P. Gütlich, A. Hauser and H. Spiering, *Angewandte Chemie International Edition in English*, 1994, **33**, 2024-2054.
49. *Pattern N° 00-033-0664, JCPDS (2000).*
50. J. F. Moulder, W. F. Stickle, P. E. Sobol and K. D. Bomben, *Handbook of X-ray photoelectron spectroscopy*, Perkin Elmer Corporation, Eden Prairie, MN, 1992.

Graphical abstract

for

An old workhorse for new applications: $Fe(dpm)_3$ as precursor for low-temperature PECVD of iron(III) oxide

G. Carraro[a,*], C. Maccato[a,*], A. Gasparotto[a], D. Barreca[b], M. Walter[c,d], L. Mayrhofer[c,d], M. Moseler[c,d], A. Venzo[b], R. Seraglia[b], C. Marega[a]

[a] *Department of Chemistry - Padova University and INSTM - 35131 Padova, Italy.*
*Corresponding authors. *E-mail:* giorgio.carraro@unipd.it (G.C.); chiara.maccato@unipd.it (C.M.).

[b] *CNR-IENI and INSTM - Department of Chemistry - Padova University - 35131 Padova, Italy.*

[c] *Fraunhofer Institute for Mechanics of Materials - 79108 Freiburg, Germany.*

[d] *Freiburg Materials Research Center - Freiburg University - 79104 Freiburg, Germany.*
E-mail: michael.walter@iwm.fraunhofer.de (M.W.).

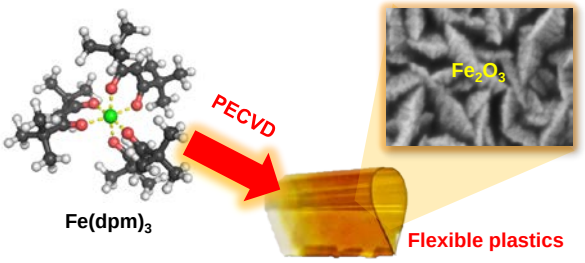

A joint theoretical-experimental investigation on $Fe(dpm)_3$ as precursor for the PECVD of iron(III) oxide is presented. Pure Fe_2O_3 nanomaterials have been obtained at temperatures as low as 100°C, even on flexible plastic substrates.